Published online: August 14, 2018

Article

SOURCE DATA | TRANSPARENT PROCESS

THE EMBO JOURNAL

DCAF13 promotes pluripotency by negatively regulating SUV39H1 stability during early embryonic development

Yin-Li Zhang[1,2,†], Long-Wen Zhao[1,†], Jue Zhang[1,†], Rongrong Le[3], Shu-Yan Ji[1], Chuan Chen[3], Yawei Gao[3], Dali Li[4], Shaorong Gao[3] & Heng-Yu Fan[1,*]

Abstract

Mammalian oocytes and zygotes have the unique ability to reprogram a somatic cell nucleus into a totipotent state. SUV39H1/2-mediated histone H3 lysine-9 trimethylation (H3K9me3) is a major barrier to efficient reprogramming. How SUV39H1/2 activities are regulated in early embryos and during generation of induced pluripotent stem cells (iPSCs) remains unclear. Since expression of the CRL4 E3 ubiquitin ligase in oocytes is crucial for female fertility, we analyzed putative CRL4 adaptors (DCAFs) and identified DCAF13 as a novel CRL4 adaptor that is essential for preimplantation embryonic development. Dcaf13 is expressed from eight-cell to morula stages in both murine and human embryos, and Dcaf13 knockout in mice causes preimplantation-stage mortality. Dcaf13 knockout embryos are arrested at the eight- to sixteen-cell stage before compaction, and this arrest is accompanied by high levels of H3K9me3. Mechanistically, CRL4-DCAF13 targets SUV39H1 for polyubiquitination and proteasomal degradation and therefore facilitates H3K9me3 removal and zygotic gene expression. Taken together, CRL4-DCAF13-mediated SUV39H1 degradation is an essential step for progressive genome reprogramming during preimplantation embryonic development.

Keywords histone methylation; maternal–zygotic transition; preimplantation embryos; protein ubiquitination; zygote

Subject Categories Chromatin, Epigenetics, Genomics & Functional Genomics; Development & Differentiation; Stem Cells

DOI 10.15252/embj.201898981 | Received 8 January 2018 | Revised 7 July 2018 | Accepted 23 July 2018

The EMBO Journal (2018) e98981

Introduction

During early preimplantation development of mammalian embryos, genomes are highly asymmetric in epigenetic modifications of DNA and of the associated chromatin and undergo dramatic reorganization (Feil, 2009). These changes participate in the establishment of stable and heritable epigenetic modifications and may occur simultaneously during development and cell differentiation (Smith & Meissner, 2013; Hatanaka *et al*, 2015). Maternal factors involved in the regulation of zygotic genome reprogramming have been extensively studied (Ancelin *et al*, 2016; Zhang *et al*, 2016). Nonetheless, these maternal factors are presumably downregulated sharply after fertilization (Lee *et al*, 2014). Therefore, by continuing and substituting the function of maternal factors, products of early responsive genes after zygotic gene activation also play key roles in reprogramming of the genomes and in the support of early development of normal and cloned embryos. With the help of advances in single-cell sequencing techniques, gene expression profiles of murine and human early embryos have been extensively studied (Hou *et al*, 2013; Xue *et al*, 2013). On the other hand, the functions and biochemical properties of these early zygotic genes have yet to be fully identified.

Mammalian oocytes and zygotes are different from somatic cells in their ability to reprogram a somatic cell nucleus into a totipotent state enabling animal cloning through somatic cell nuclear transfer (SCNT) (Lu & Zhang, 2015). Nonetheless, the majority of SCNT embryos fail to develop to term because of undefined reprogramming defects (Niemann, 2016). SUV39H1-mediated histone H3 lysine-9 trimethylation (H3K9me3) of the donor cell genome is a major barrier to efficient reprogramming by SCNT. Removal of this epigenetic mark either through ectopic expression of an H3K9me3-specific demethylase, KDM4D or KDM5B, in oocytes or through a knockdown of the H3K9 methyltransferases (SUV39H1/2) in donor cells not only attenuates the zygotic gene activation defect but also greatly improves the reprogramming efficiency of SCNT (Matoba *et al*, 2014; Liu *et al*, 2016). Nevertheless, it remains unclear how the SUV39H1/2 activities are disabled in early embryos derived from normal fertilization or in the process of induced pluripotent stem cell (iPSC) reprogramming.

1 Life Sciences Institute, Zhejiang University, Hangzhou, China
2 Assisted Reproduction Unit, Department of Obstetrics and Gynecology, Sir Run Run Shaw Hospital, School of Medicine, Zhejiang University, Hangzhou, China
3 Clinical and Translational Research Center of Shanghai First Maternity & Infant Hospital, School of Life Sciences and Technology, Tongji University, Shanghai, China
4 Shanghai Key Laboratory of Regulatory Biology, Institute of Biomedical Sciences and School of Life Sciences, East China Normal University, Shanghai, China
*Corresponding author. Tel: +86-571-88981370; E-mail: hyfan@zju.edu.cn
†These authors contributed equally to this work

© 2018 The Authors

CRL4 ubiquitin E3 ligase in oocytes is crucial for female fertility. Oocyte-specific deletion of damaged DNA-binding protein 1 (DDB1)—the linker protein of the CRL4 complex—causes rapid primordial follicle loss and premature ovarian insufficiency (Yu *et al*, 2013, 2015b). CUL4, one of three founding cullins conserved from yeast to humans, uses DDB1 as a linker to interact with a subset of WD40-repeat-containing DDB1/CUL4-associated factors (DCAFs) that serve as substrate receptors, forming as many as 90 E3 complexes (Lee & Zhou, 2007). Among these, DCAF1 has been identified as a major maternal substrate adaptor of CRL4 that maintains oocyte survival (Yu *et al*, 2013). $CRL4^{DCAF1}$ regulates expression of genes essential for oocyte survival and ovulation in primordial follicles and for paternal DNA demethylation upon fertilization, partially by modulating TET1/2/3 activities through monoubiquitination of a conserved lysine site to regulate DNA methylation levels in oocytes (Yu *et al*, 2013). Nonetheless, *Ddb1*-null embryos have more severe developmental defects than *Tet3*-null embryos (Gu *et al*, 2011), indicating that CRL4 supports early embryonic development by additional mechanisms.

In this study, we report DCAF13 as a novel CRL4 adaptor that is essential for preimplantation embryonic development. *Dcaf13* is an early zygotic gene in both murine and human embryos and is expressed mainly at eight-cell to morula stages. *Dcaf13* knockout murine embryos are arrested at the eight- to sixteen-cell stage before compaction, and this situation causes preimplantation mortality. Mechanistically, $CRL4^{DCFA13}$ directs SUV39H1/2 to polyubiquitination and proteasomal degradation and thereby triggers histone H3 lysine-9 demethylation and zygotic genome reprogramming.

Results

DCAF13 is a conserved DDB1/CUL4-associated factor that is specifically induced in early embryos

By analyzing the expression profile of 14 DCAFs detected in human oocytes and early embryos by single-cell RNA sequencing (Hou *et al*, 2013; Yan *et al*, 2013), we noticed that DCAF13, a putative CRL4 substrate adaptor, was an early zygotic gene whose expression was specifically induced as early as the four- to eight-cell stage (Fig 1A). Quantitative RT–PCR and data from RNA-seq datasets (GSE70605) in mouse oocytes and early embryos both showed that murine *Dcaf13* mRNA was also transiently expressed during four-cell to morula stages, in comparison with other DCAFs (Fig EV1A and B). Western blot and immunofluorescence results showed that DCAF13 was expressed as early as the four-cell stage and continued to accumulate in morulae and blastocysts (Fig 1B and C). Moreover, DCAF13 was mainly located in the nucleoli of blastomeres from four-cell to blastocyst stages, as indicated by its co-localization with well-established nucleolar marker B23 (also known as NPM1; Fig 1C). Furthermore, DCAF13 was uniformly distributed in trophectoderm cells and inner cells mass, which was indicated by co-staining of CDX2 and DCAF13 in mouse blastocyst embryos (Fig EV1C).

The *Dcaf13* gene is conserved from yeast to mammals, but its function has not been identified in any species. We cloned the mouse *Dcaf13* cDNA from a mouse ovary cDNA pool (Yu *et al*, 2016). It encodes a highly conserved protein of 445 amino acid residues with a molecular weight of 52 kDa; this protein contains seven WD40 repeats at the N terminus and a SOF1 domain at the C terminus (Appendix Fig S1). Co-immunoprecipitation results in HeLa cells indicated that DCAF13 interacts with CRL4 linker protein DDB1; the DCAF13–DDB1 interaction was abrogated by WD domain deletion but was strengthened by SOF1 domain deletion (Fig EV2A and B).

We also examined the subcellular localization of DCAF13 in somatic cells. Both overexpressed FLAG-DCAF13 and endogenous DCAF13 were co-localized with B23 and were enriched in nucleoli of HeLa cells and MEFs (Fig EV2C and D). Deletion of the SOF1 domain, but not WD40 repeats, abrogated the nucleolar localization of DCAF13 (Fig EV2C). This result is in agreement with other reports, which show that the SOF1 domain mediates protein–RNA interactions in the yeast nucleolus (Jansen *et al*, 1993; Bax *et al*, 2006).

DCAF13 is crucial for early embryonic development in mice

To elucidate the function of DCAF13 in mice, we generated *Dcaf13* knockout mouse strains using a TALEN-based gene targeting approach. Two independent strains containing frame shift mutations at an *Alu* I restriction site within *Dcaf13* exon 2 were obtained and analyzed (Fig EV3A and B). For both strains, when $Dcaf13^{+/-}$ males and females were crossed, the ratio of newborn $Dcaf13^{+/+}$, $Dcaf13^{+/-}$, and $Dcaf13^{-/-}$ pups was close to 1:2:0. The 8-bp deletion *Dcaf13* mutant strain was used in all of the following experiments. We examined genotypes of the embryos from day postcoitus (dpc) 8.5 to dpc 16.5 and did not find any $Dcaf13^{-/-}$ embryos (Fig 2A). At dpc 3–4, *Dcaf13* knockout embryos were identified by DNA genotyping (Fig EV3C) and DCAF13 immunofluorescence (Fig 2B). These embryos were morphologically normal up to the eight-cell stage; however, they did not compact, failed to develop into blastocysts, and died at the morula stage. Notably, the nucleolar B23 signals were also weakened in $Dcaf13^{-/-}$ embryos (Fig 2B). These results indicate that the *Dcaf13* knockout causes early embryonic death.

Because $Dcaf13^{-/-}$ embryos were obtained in small numbers and could not be identified for detailed analyses before processing for genotyping, we employed an RNA interference (RNAi) approach to assess DCAF13 function in preimplantation development, by injecting *Dcaf13*-targeting small interfering RNAs (siRNAs) into the cytoplasm of wild-type (WT) zygotes. An immunofluorescence assay revealed that DCAF13 was greatly downregulated in siRNA-injected embryos at the eight-cell stage (Fig 2C). Just as the $Dcaf13^{-/-}$ embryos, most *Dcaf13* knockdown embryos failed to undergo compaction and showed developmental arrest at the morula stage (Fig 2D and E).

$CRL4^{DCAF13}$ regulates histone H3 lysine-9 methylation and heterochromatin by targeting SUV39H1 for polyubiquitination and degradation

Because murine preimplantation embryos are inconvenient for extensive biochemical analyses, we studied biochemical functions of DCAF13 primarily in HeLa cells and MEFs and then verified the results in murine preimplantation embryos. The DCAF13

 © 2018 The Authors

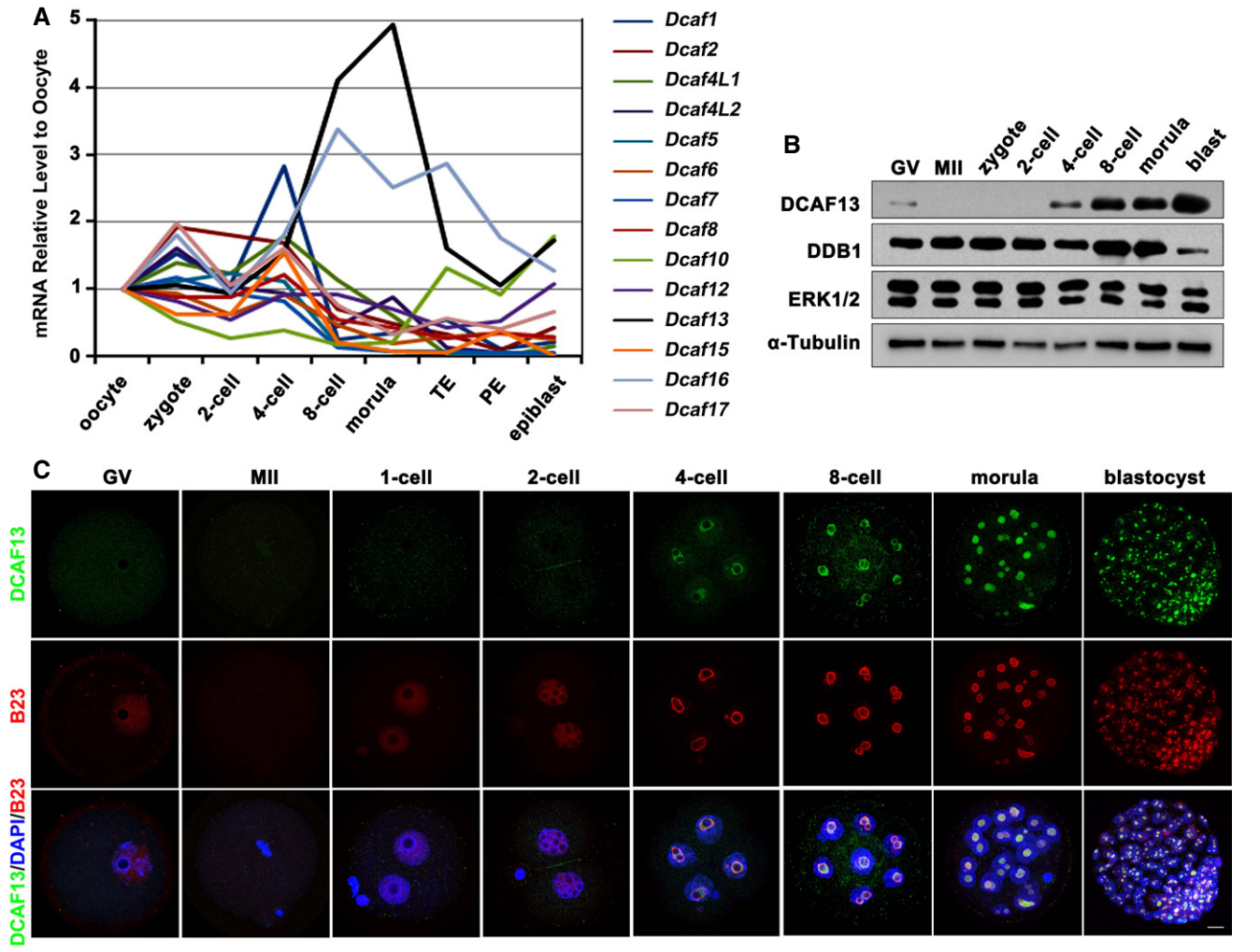

Figure 1. ***Dcaf13*** **is a gene zygotically expressed early during human and murine embryonic development.**

A mRNA profiles of 14 DCAFs detected in human oocytes and early embryos by RNA-seq. The relative mRNA level in germinal vesicle (GV) stage oocytes was set to 1.0, and fold changes at different stages are shown. TE, trophectoderm; PE, primitive endoderm.

B Western blotting of DCAF13 and DDB1 in mouse oocytes and preimplantation embryos. ERK1/2 and α-tubulin were immunoblotted as loading controls. Total protein samples from 100 oocytes or embryos were loaded onto each lane.

C Confocal microscopic images of DCAF13 (green) and B23 (red) immunofluorescence in mouse oocytes and preimplantation embryos. DNA was counterstained with 4′,6-diamidino-2-phenylindole (DAPI, blue). At each stage, more than 30 oocytes or embryos were examined, with similar results. Scale bar = 10 μm.

Source data are available online for this figure.

knockdown by RNAi inhibited proliferation and colony growth in HeLa cells (Fig 3A). Nonetheless, these cells tested negative for apoptotic marker cleaved caspase 3 or DNA damage marker pH2AX, indicating that DCAF13 depletion did not cause growth retardation by inducing programmed cell death (Fig EV4A–C). DCAF13-depleted cells were first identified by negative DCAF13 staining (Fig 3B). They changed their shape from flat to round and showed dense DNA staining as well as increased histone H3 trimethylation at lysine-9 (H3K9me3, a heterochromatin marker, Fig 3B and C, circled by dotted lines). Being related to the H3K9me3 upregulation, H3K9me2 levels were also slightly increased, but H3K9 acetylation (H3K9ac) was only mildly decreased after the DCAF13 knockdown (Fig EV4D–F). In contrast, other histone modifications, for example, H2A-K119 monoubiquitination, (H2A-K119ub1) were unaffected (Fig EV4G). Interestingly, H3K27me3 was slightly increased after the *Dcaf13* knockdown (Fig EV4H and I).

In addition to H3K9me3, both DCAF13- and DDB1-depleted cells showed increased levels of heterochromatin protein 1α (HP1α) and H3K9 methyltransferase SUV39H1 (Fig 3D). Going back to the *in vivo* system, we also found that H3K9me3 and SUV39H1 were remarkably upregulated and deposited clearly at the nuclear periphery and nuclear particles in DCAF13 knockdown eight- to sixteen-cell embryos (Fig 3E and F). Previous mass spectrometry results have shown that DCAF13 interacts with SUV39H1 (Yang *et al*, 2015). Therefore, we hypothesized that $CRL4^{DCAF13}$ regulates histone H3K9

© 2018 The Authors

A

dpc	No. of progenies		
	+/+	+/–	–/–
E4.5	8	24	9
E8.5	3	7	0
E10.5	6	13	0
E12.5	4	7	0
E14.5	8	17	0
E16.5	4	8	0
After birth	117	224	0

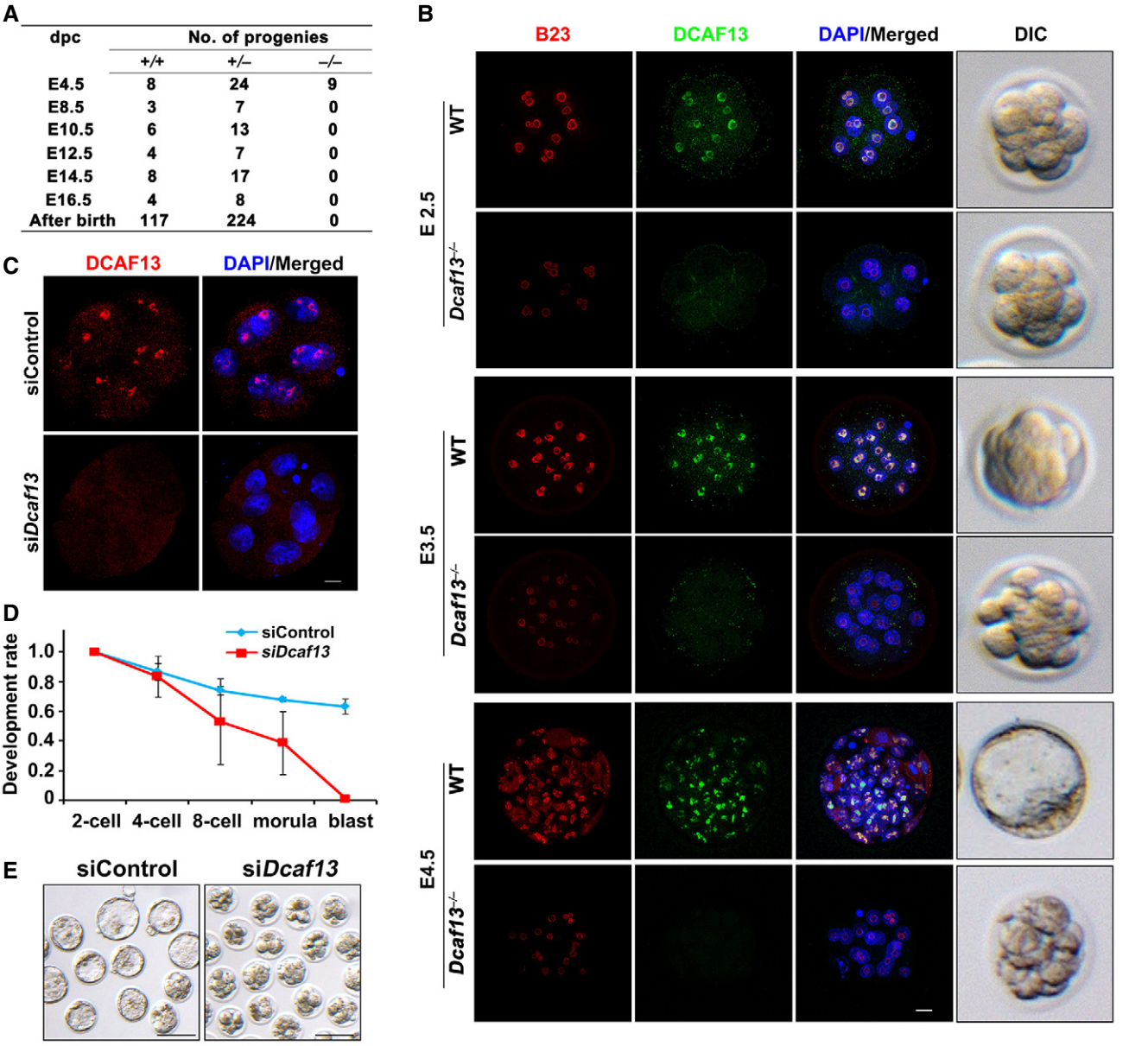

Figure 2. DCAF13 is essential for murine preimplantation embryonic development.

A Genotyping results on *Dcaf13*$^{+/+}$, *Dcaf13*$^{+/-}$, and *Dcaf13*$^{-/-}$ mouse embryos and offspring. Note that no *Dcaf13*$^{-/-}$ embryos or pups were obtained at or after 8.5 dpc.

B DCAF13 (green) and B23 (red) immunofluorescence in embryos at E2.5, E3.5, and E4.5 collected from *Dcaf13*$^{+/-}$ female mice mated with adult *Dcaf13*$^{+/-}$ male mice. DIC images were taken from the same batch of embryos before fixation and immunofluorescence. The embryos were genotyped after the DIC images were taken in order to assign them as either wild type or mutant. n = 4 mice at each time point. Scale bars = 10 μm.

C DCAF13 immunofluorescence in eight-cell WT embryos, which were microinjected with *Dcaf13* siRNAs (*siDcaf13*) or control siRNAs (*siControl*). n = 25 embryos for each group. Scale bars = 10 μm.

D *In vivo* fertilized eggs were collected from oviducts, microinjected with *siControl* (n = 91) or *siDcaf13* (n = 117), and then cultured for 72 h *in vitro*. The percentage of embryos that reached two-cell, four-cell, eight-cell, morula, and blastocyst stages at 48, 60, 72, 84, and 96 h post-hCG (human chorionic gonadotropin) injection were calculated and presented as developmental rate. Error bars indicate mean ± SD.

E Representative images showing the development of preimplantation embryos at E4.5, with or without the *Dcaf13* knockdown. Scale bars = 100 μm.

trimethylation and chromatin conformation changes by targeting SUV39H1.

Co-immunoprecipitation results revealed that DCAF13 and DDB1 interacted with SUV39H1 (Fig 4A) and its homolog SUV39H2 (Appendix Fig S2A and B). Overexpression of DCAF13 or DDB1 significantly increased the polyubiquitination of SUV39H1 (Fig 4B) and SUV39H2 (Appendix Fig S2C). Conversely, when endogenous DCAF13 or DDB1 was depleted by siRNAs, SUV39H1 polyubiquitination was decreased (Fig 4C). We analyzed the degradation rates of SUV39H1 in cells cultured in the presence of cycloheximide (CHX), a protein

 © 2018 The Authors

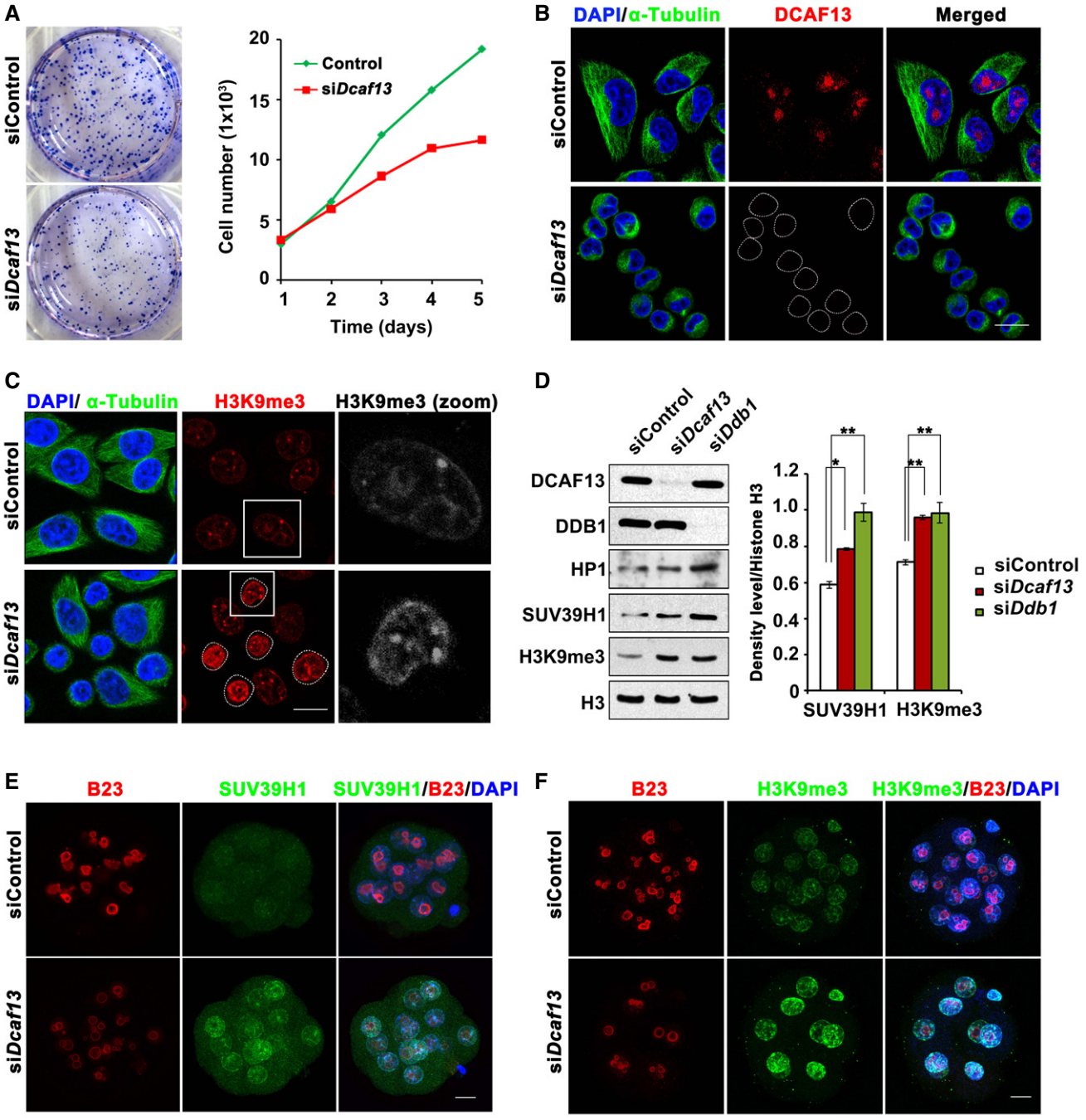

Figure 3. DCAF13 regulates H3K9me3 and SUV39H1 levels in HeLa cells and preimplantation embryos.

A Images of colony formation and proliferation rates of HeLa cells with or without *Dcaf13* knockdown. Proliferation rates were determined by a CCK8 proliferation assay (n = 5). Optical density at 450 nm (OD_{450}) values was converted to cell numbers.

B DCAF13 immunofluorescence (red) in control and *Dcaf13* knockdown HeLa cells co-stained with α-tubulin (green) and DAPI (blue). DCAF13-negative cells are circled by dotted lines. Scale bar = 10 μm.

C H3K9me3 immunofluorescence in control and *Dcaf13* knockdown HeLa cells. DCAF13 knockdown cells are circled by dotted lines. The white box around the nucleus showing H3K9me3 signal was zoomed out on the right panel. Three independent experiments were conducted. Scale bar = 10 μm.

D Western blot analysis of the indicated proteins in control and *Dcaf13* or *Ddb1* knockdown cells. Histone H3 was immunoblotted as a loading control. Three independent experiments were performed in HeLa cells. The intensity of SUV39H1 and H3K9me3 relative to histone H3 quantified in ImageJ software was calculated and shown as mean ± SD. $^{**}P < 0.01$; $^{*}P < 0.05$, calculated by two-tailed Student's t-test.

E, F SUV39H1 (E) and H3K9me3 (F) immunofluorescence in eight- to sixteen-cell embryos, which were microinjected with control or *Dcaf13* siRNA at the zygote stage. The nucleolar protein B23 was co-stained as an immunofluorescence marker. DNA was labeled by DAPI. At least 30 embryos in each group were examined and showed similar results. Scale bars = 10 μm.

Source data are available online for this figure.

© 2018 The Authors

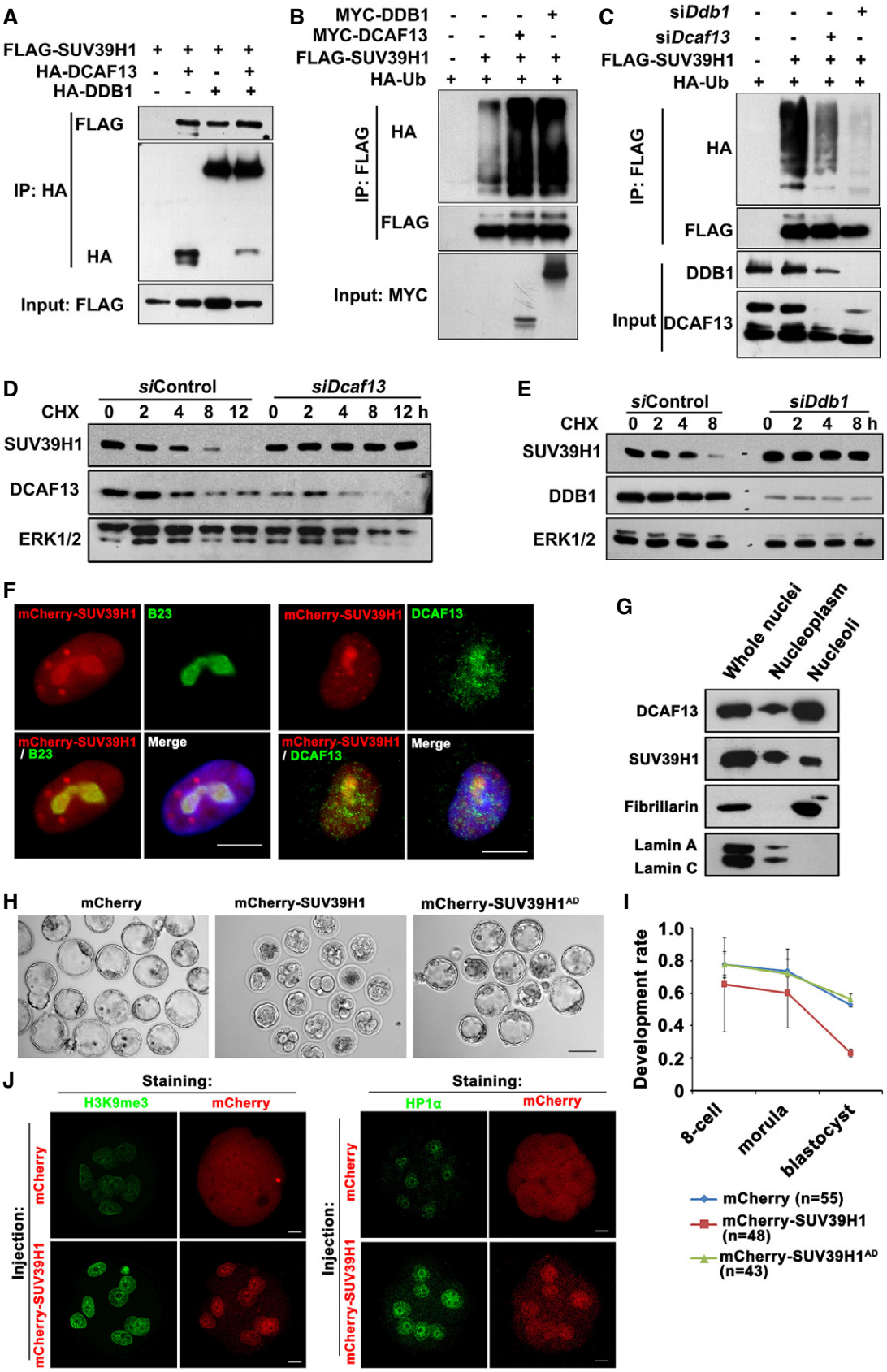

Figure 4.

© 2018 The Authors

Figure 4. $CRL4^{DCAF13}$ targets SUV39H1 for polyubiquitination and degradation.

A, B Co-immunoprecipitation (Co-IP) experiments showing interactions of SUV39H1 with DDB1-DCAF13 (A) and SUV39H1 polyubiquitination (B). HeLa cells transiently transfected with plasmids encoding the indicated proteins were lysed and subjected to IP with an anti-HA affinity gel. Input cell lysates and precipitates were immunoblotted with antibodies against FLAG, HA, and MYC.

C IP followed by Western blotting showing SUV39H1 polyubiquitination in control HeLa cells and those transfected with *Dcaf13* or *Ddb1* siRNAs.

D, E Cycloheximide (CHX)-chasing experiments showing SUV39H1 stability. HeLa cells transfected with control, *Dcaf13* (D), or *Ddb1* siRNAs (E) were treated with 100 μg/ml CHX to inhibit *de novo* protein synthesis. At the indicated time points after the CHX treatment, the cells were lysed for immunoblotting. The relatively stable proteins ERK1 and ERK2 were immunoblotted as an internal control.

F HeLa cells were transfected with expression plasmids encoding mCherry or mCherry-SUV39H1 and were fixed for immunofluorescent staining with nucleoli marker B23 (left panels) or DCAF13 (right panels) 24 h later. Nuclei were stained with DAPI. Scale bar = 10 μm.

G The nuclei, nucleoli, and nucleoplasm of HeLa cells were isolated and subjected to immunoblot with DCAF13, SUV39H1, fibrillarin, and lamin A/C. The result shows that both DCAF13 and SUV39H1 have nuclear and nucleolar localization.

H Representative embryo images at E4.5. Zygotes were microinjected with mRNAs encoding mCherry (as control), mCherry-SUV39H1, or mCherry-$SUV39H1^{AD}$ (inactive) and cultured for 4 days. Scale bar = 100 μm.

I Developmental rates of embryos microinjected with mRNAs encoding WT or mutated SUV39H1 as in (H). The numbers of eight-cell embryos, morulae, and blastocysts were counted at E2.5, E3, and E4.5, respectively. Error bars represent mean ± SD of three independent experiments.

J Immunofluorescence of H3K9me3 and HP1α in eight-cell embryos that were microinjected with mRNAs encoding mCherry or mCherry-SUV39H1 at the zygote stage. Scale bars = 10 μm.

Source data are available online for this figure.

synthesis inhibitor. The SUV39H1 protein was mostly degraded within 8 h after CHX treatment but was stabilized in DCAF13- or DDB1-depleted cells (Fig 4D and E). In HeLa cells transfected with a mCherry-tagged SUV39H1, immunofluorescence assay results suggested that mCherry-SUV39H1 and DCAF13 can be detected in the entire nucleus, but the signal in nucleolus is much stronger than that in the nucleoplasm (Fig 4F). Furthermore, we separated proteins in nucleoplasm and nucleoli and detected the presence of DCAF13 and SUV39H1. Fibrillarin and lamin A/C were blotted as marker proteins of nucleoli and nucleoplasm, respectively (Fig 4G). Endogenous DCAF13 and SUV39H1 were present in both fractions, but DCAF13 was more abundant in nucleoli than in nucleoplasm (Fig 4G). Endogenous SUV39H1 did not show an enrichment in nucleolus as the overexpressed mCherry-SUV39H1 detected in Fig 4F. This might be caused by the differences in intracellular SUV39H1 abundance. These results provide evidence that SUV39H1 is an accessible substrate of DCAF13.

$CRL4^{DCAF13}$-mediated SUV39H1 degradation is necessary for preimplantation embryonic development

Next, we tested whether impaired SUV39H1 degradation contributed to the early embryonic death caused by *Dcaf13* deletion. Microinjection of mRNAs encoding SUV39H1, but not a catalytic-activity-dead SUV39H1 mutant (NHSC residues in the catalytic domain were mutated to NLAA, $SUV39H1^{AD}$; Rea *et al*, 2000), into mouse zygotes, significantly decreased their rates of development into blastocysts (Fig 4H and I). Overexpression of SUV39H1 also increased H3K9me3 and HP1α levels in blastomeres at the eight-cell stage (Fig 4J). These phenotypic features were similar to those caused by DCAF13 depletion in early embryos.

Furthermore, we determine whether SUV39H1 knockdown rescues the growth defect phenotype caused by DCAF13 depletion. However, the results showed that *Suv39h1* knockdown failed to rescue the developmental arrest in preimplantation embryos after DCAF13 depletion (Fig EV5A and B). It is conceivable that DCAF13 may have substrates other than SUV13H1 in regulating preimplantation development, such as some proteins involved in nucleolus functions. In addition, quantitative RT–PCR results showed that the efficiency of *Suv39h1* knockdown by siRNA microinjection was much higher in *Dcaf13*-depleted embryos than in control embryos (Fig EV5C and D). Therefore, it is likely that the control level of SUV39H1 protein is indispensable for preimplantation development and that the developmental failure would occur when *Suv39h1* siRNA efficiently eliminated SUV39H1 protein into the level much lower than the control.

Because histone modifications are known to affect transcription of a wide range of genes in many cell types, we analyzed the transcription changes caused by DCAF13 depletion in embryos at twelve- to sixteen-cell stages when the phenotype of the *Dcaf13* knockout or knockdown becomes noticeable. To label the newly synthesized RNAs, 5-ethynyl uridine (EU) was added to the medium 2 h before fixation of control and *siDcaf13* embryos. Strong EU signals were detected around nucleoli in control embryos (Fig 5A and B). This observation is consistent with other reports, which show that ribosomal RNAs are transcribed early and abundantly in preimplantation embryos (Yan *et al*, 2013; Jiang *et al*, 2014). In contrast, the nucleolar EU signals significantly decreased in DCAF13-depleted (Fig 5A) and SUV39H1-overexpressing (Fig 5B; Appendix Fig S3A) embryos. The EU signal in eight-cell embryos with injection of mCherry-SUV39H1 was significantly decreased compared with that in mCherry-overexpressed embryos, especially around the nucleolus (Appendix Fig S3A–C).

To determine whether DCAF13 and SUV39H1 are involved in the control of rDNA transcription in preimplantation embryos, we examined the amount of 45S pre-rRNA by RT–PCR using primers amplifying its 3′-external transcriptional spacer (3′-ETS). In agreement with the EU staining results, pre-rRNA levels were low in both DCAF13-depleted and SUV39H1-overexpressing embryos (Fig 5C and D). We also used ultra-low-input native chromatin immunoprecipitation (ULI-NChIP; Brind'Amour *et al*, 2015) to test whether DCAF13 depletion led to increased H3K9 trimethylation at the rDNA loci. Primers targeting different regions of mouse and human rDNA were used for RT–PCRs (Fig 5E and F, and Appendix Fig S4A). The results showed that H3K9me3 levels in the 5′-ETS, 18S, and intergenic spacer (IGS) loci in DCAF13-depleted embryos were significantly higher than those in control embryos (Fig 5F). In HeLa cells, *Dcaf13* depletion also caused H3K9me3 accumulation at the H0 and H8 locus of human rDNA region, whereas co-depletion of *Suv39h1*

© 2018 The Authors

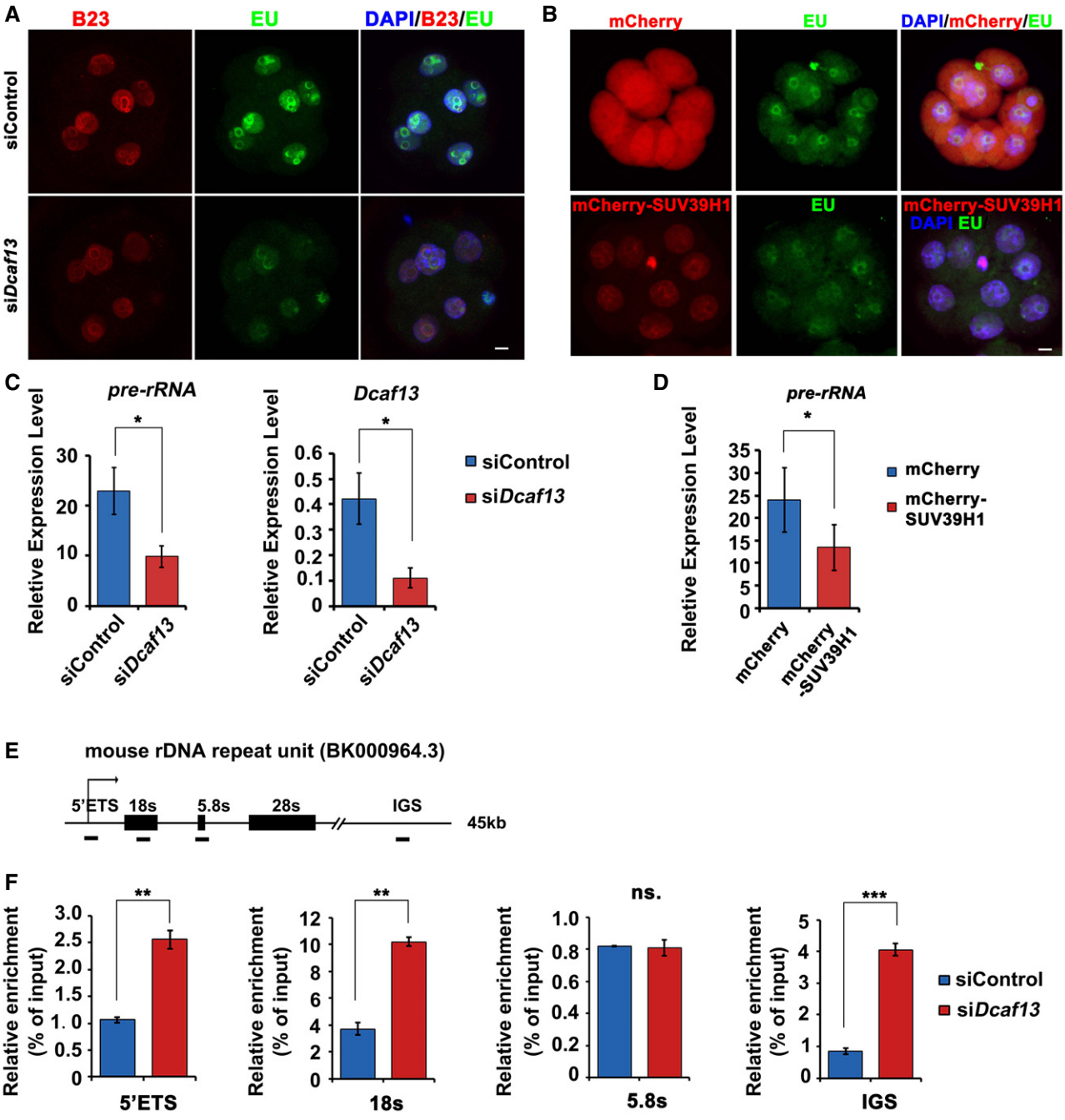

Figure 5. DCAF13 depletion and SUV39H1 overexpression affect rDNA transcription.

A 5-Ethynyl uridine (EU) fluorescence showing RNA transcription in eight- to twelve-cell embryos that were microinjected with siControl or *siDcaf13* at the zygote stage. B23 was co-stained to label the nucleolus. n = 28 embryos. Scale bar = 10 μm.

B EU fluorescence showing RNA transcription in eight-cell embryos that were microinjected with mRNAs encoding mCherry or mCherry-SUV39H1 at the zygote stage. n = 35 embryos. Scale bar = 10 μm.

C, D qRT–PCR showing the decreased 45S pre-rRNA transcription in *Dcaf13* knockdown (C) or mCherry-SUV39h1-overexpressing (D) embryos at the eight-cell stage relative to controls. The RNAi efficiency was monitored by detecting *Dcaf13* mRNA relative levels (C, right panel); n = 3 biological replicates. Data are shown as mean ± SEM; $^{**}P < 0.01$; $^{*}P < 0.05$, calculated by two-tailed Student's t-test.

E Diagrams of mouse rDNA repeat unit (GenBank: BK000964.3) with general domain and the position of ChIP-qPCR primers.

F Embryos injected with control or *Dcaf13* siRNA were subjected to ULI-NChIP using H3K9me3 antibody. The enrichment of H3K9me3 on rDNA locus was determined by qPCR with indicated primers at four positions (5′ETS, 18s, 5.8s, and IGS) and normalization to 10% input DNA. One hundred eight-cell embryos were collected for each group, and results are shown of two independent experiments. Error bars, mean ± SEM. ns. $P > 0.05$; $^{**}P < 0.01$; $^{***}P < 0.001$ by two-tailed Student's t-test.

Source data are available online for this figure.

© 2018 The Authors

relieved the effect of *siDcaf13* (Appendix Fig S4B and C). The efficiency of DCAF13 and SUV39H1 depletion in HeLa cells was detected by Western blot and qRT–PCR (Appendix Fig S4D and E). Collectively, these results indicated that DCAF13 promotes rDNA transcription by balancing SUV39H1-mediated H3K9 trimethylation in preimplantation embryos.

DCAF13 ensures the appropriate expression of genes essential for cell fate commitment in preimplantation embryos

Because *Dcaf13*-deficient embryos failed to develop into a blastocyst, we suspected that DCAF13 regulates expression of genes necessary for cell fate commitment in preimplantation embryos. Although major ZGA occurs at two-cell stage in mouse embryos, not all "early zygotic genes" are started to be expressed as early as two-cell stages. For example, *Cdx2*, *Nanog*, and *Oct4* are well-recognized to be essential early zygotic genes. Their expression was detected as early as four-cell stage and gradually increased during the development from eight-cell to blastocyst stage. This time frame overlaps with the window of DCAF13 expression. Therefore, we determined expression levels of *Cdx2*, *Nanog*, and *Oct4* mRNAs in WT and *Dcaf13*$^{-/-}$ eight-cell embryos by single-embryo RT–PCR assays. *Cdx2* was greatly downregulated in *Dcaf13*$^{-/-}$ embryos, while the expression levels of *Nanog* and *Oct4* were unaffected at this stage (Fig 6A).

In addition, RT–PCR analyses of control and RNAi embryos were performed at eight-cell and morula stages. After *Dcaf13* RNAi, *Cdx2* expression levels were significantly decreased (Fig 6B), but *Oct4* expression was not affected. DCAF13 depletion did not affect *Nanog* expression at the eight-cell stage but caused a dramatic decrease in its mRNA levels at the morula stage (Fig 6B). Immunofluorescence assay results suggested that CDX2 and NANOG protein levels decreased in DCAF13 knockdown eight- to sixteen-cell embryos, with OCT4 unaffected (Fig 6C). The levels of these three proteins then increased in control blastocysts, but the DCAF13-depleted embryos were arrested at eight- to sixteen-cell stages and showed lower expression levels of these cell fate-determining factors.

Overexpression of SUV39H1 by mRNA microinjection into zygotes also caused a significant decrease in *Cdx2* mRNA expression at the eight-cell stage, as detected by qRT–PCR (Fig 6D). Collectively, DCAF13 depletion and SUV39H1 upregulation impaired the expression of early zygotic genes that are crucial for cell fate determination, especially *Cdx2*.

In addition, some other genes were expressed early in preimplantation mouse embryos, including *Sumo2*, *Kdm4b*, *Tbx20,* and *Dcaf13* itself. Significant increases in their transcription levels were detected between four-cell and morula stages (Fig 7A–D). However, their expression after major ZGA, particularly at eight-cell and morula stages, was remarkably compromised by *Dcaf13* depletion (Fig 7A–D).

Discussion

In this study, we demonstrate that CRL4^{DCAF13} regulates SUV39H1 stability by polyubiquitination and plays a key role in the establishment of pluripotency during preimplantation development. Various studies have shown that dynamic methylation and demethylation of histone H3 lysine-4 are essential for early embryonic development, and H3K9me3 is a major barrier to somatic genome reprogramming during SCNT (Chen *et al*, 2013; Yu *et al*, 2015b; Liu *et al*, 2016). Several members of the KDM family of histone demethylases remove H3K9me3 from genomic heterochromatin regions during normal or engineered embryonic development, to ensure proper cell fate commitment and differentiation (Chung *et al*, 2015; Herberg *et al*, 2015). Nevertheless, it is unclear whether there are specific zygotic factors that directly repress or remove SUV39H1 activity in early embryos. Experimental evidence indicated that SUV39H1 depletion in donor somatic cells by RNAi significantly increased the developmental rates of SCNT embryos (Matoba *et al*, 2014), indicating that there must be an endogenous factor in recipient zygotes that downregulates SUV39H1. Our results indicate that DCAF13 is a strong candidate for this zygotic factor that represses SUV39H1-mediated H3K9 trimethylation.

DCAF13 is not the only factor that mediates SUV39H1 polyubiquitination and degradation. It has been reported that the H3K9me3-repressive histone conformation of p53's target promoters is abrogated in response to p53 activation by transformed mouse 3T3 cell double minute 2 (MDM2)-mediated SUV39H1 degradation (Bosch-Presegue *et al*, 2011). On the other hand, p53 activity is repressed in early blastomeres (Ziegler-Birling *et al*, 2009; Ma *et al*, 2013). Besides, MDM2 has targets other than SUV39H1, many of them are essential for cell survival and proliferation; activation of MDM2-mediated protein degradation is intolerable for preimplantation embryos (Yang *et al*, 2006; Zhu *et al*, 2009). Therefore, this DCAF13-dependent mechanism is likely to play a major role in the removal of SUV39H1 in preimplantation embryos.

Some reports have predicted DCAF13 as a putative CRL4 substrate adaptor (Jin *et al*, 2006). Nonetheless, the interaction of DCAF13 with CRL4 core subunits has not been experimentally demonstrated until our present study. *Dcaf13* is an ancient gene that exists in many species, from yeast to humans, and its encoded protein sequences are highly conserved. To our surprise, the biochemical and physiological functions of DCAF13 have never been specifically explored. There was only one study that identified non-synonymous polymorphisms in the *Dcaf13* gene (also known as *Wdsof1*) as novel susceptibility markers for low bone mineral density in Japanese postmenopausal women (Urano *et al*, 2010). Our experiments have shown that CRL4 subunits and its well-established substrate adaptor DCAF1 are highly expressed in mouse oocytes. A maternal *Ddb1* or *Dcaf1* knockout caused developmental arrest of the zygotes immediately after fertilization (Yu *et al*, 2013, 2015a). In contrast, the DCAF13 expression level is low in oocytes and zygotes, but promptly increases during the four- to eight-cell stage in human and mouse embryos. In line with the *Dcaf13* expression pattern, zygotic *Dcaf13* knockout embryos showed defects as early as the eight-cell stage (no embryo compaction) and were arrested and died at the morula stage. On the basis of these new findings, we added *Dcaf13* to the list of essential mammalian zygotic genes that are genetically confirmed. Notably, *Dcaf13* is the only CRL4 substrate adaptor-encoding gene that fits into this category.

Both yeast and human DCAF13s are nucleolar proteins. The conserved SOF1 domain at DCAF13's C terminus mediates the nucleolar localization (Jansen *et al*, 1993; Bax *et al*, 2006). We found that the SOF1 domain deletion not only caused DCAF13 translocation to the cytoplasm but also strengthened the binding

© 2018 The Authors

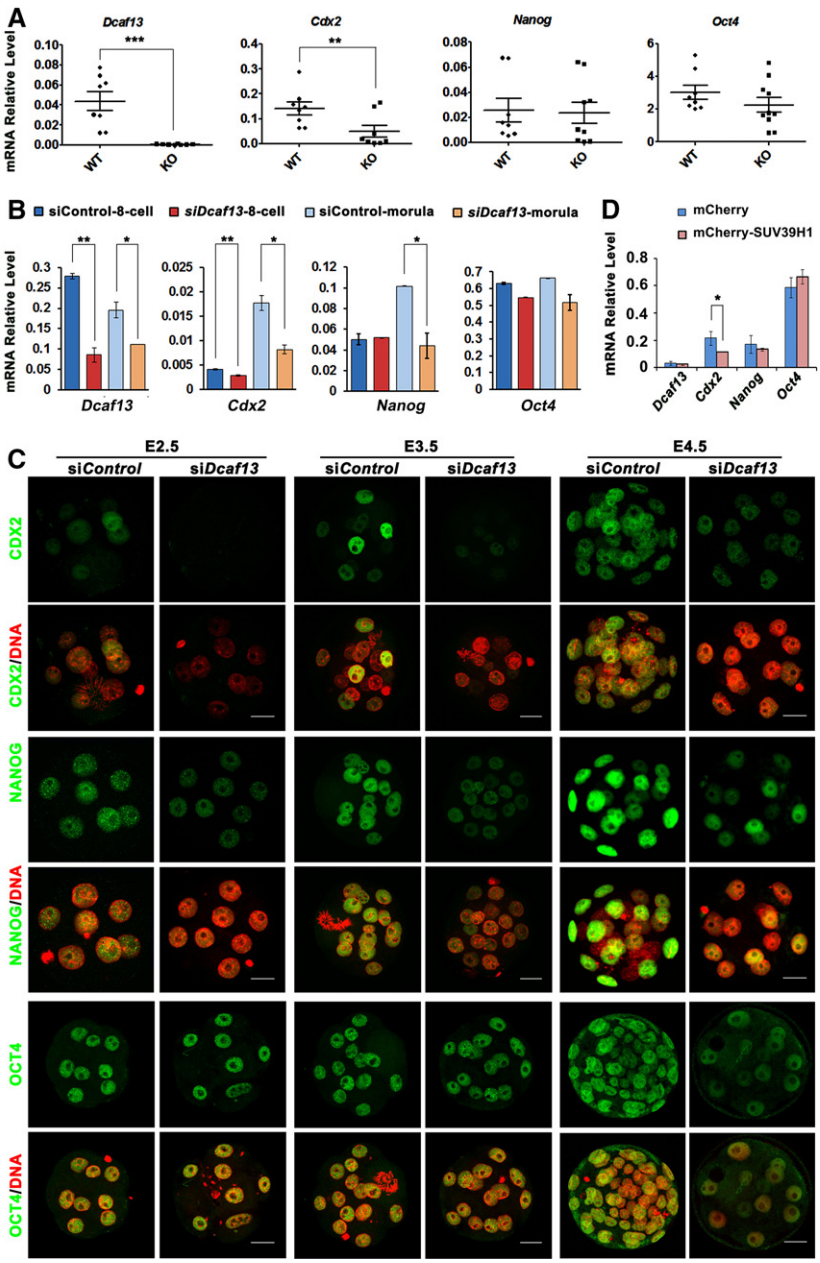

Figure 6. DCAF13 and SUV39H1 regulate *Cdx2* and *Nanog* expression in preimplantation embryos.

A Single-embryo qRT–PCR analysis of selected genes (*Dcaf13*, *Cdx2*, *Nanog*, and *Oct4*) in WT and *Dcaf13*$^{-/-}$ embryos at eight-cell stages. Each dot represents a signal embryo. Data are shown as mean ± SEM. Significance was calculated by Student's *t*-test: ***$P < 0.001$; **$P < 0.01$.

B qRT–PCR analysis of selected genes (*Dcaf13*, *Cdx2*, *Nanog*, and *Oct4*) in eight-cell embryos and morulae that were microinjected with control or *Dcaf13* siRNAs. The mRNA relative levels were normalized to *Gapdh* and are shown as mean ± SEM. Fifty embryos were collected for each time point. Significance was calculated by Student's *t*-test: **$P < 0.01$; *$P < 0.05$.

C Immunofluorescence of CDX2, NANOG, and OCT4 in control and *siDcaf13* embryos at E2.5, E3.5, and E4.5, which is the time point that the control embryos develop to eight-cell, morula, and blastocyst stages. At least 30 embryos were observed in each experimental group and three independent experiments were conducted. Scale bars = 10 μm.

D qRT–PCR analysis of *Dcaf13*, *Cdx2*, *Nanog*, and *Oct4* in eight-cell embryos overexpressed mCherry or mCherry-SUV39H1. The relative mRNA levels were normalized to *Gapdh*, which is used as an internal control. Data are shown as mean ± SEM. Significance was calculated by Student's *t*-test. *$P < 0.05$.

between DCAF13 and DDB1. This result indicates that the CRL4–DCAF13 interaction is dynamic and affected by DCAF13 location. The potential role of CRL4 in the nucleolus has never been reported. Among the core CRL4 subunits, CUL4A is mainly a cytoplasmic protein, whereas CRL4B, DDB1, and ROC1 are enriched in the nucleus in most cell types being studied (Pan *et al*, 2013; Hannah & Zhou, 2015; Jia *et al*, 2017). Within the nucleus, these three CRL4 subunits are distributed in both the nucleolus and nucleoplasm.

 © 2018 The Authors

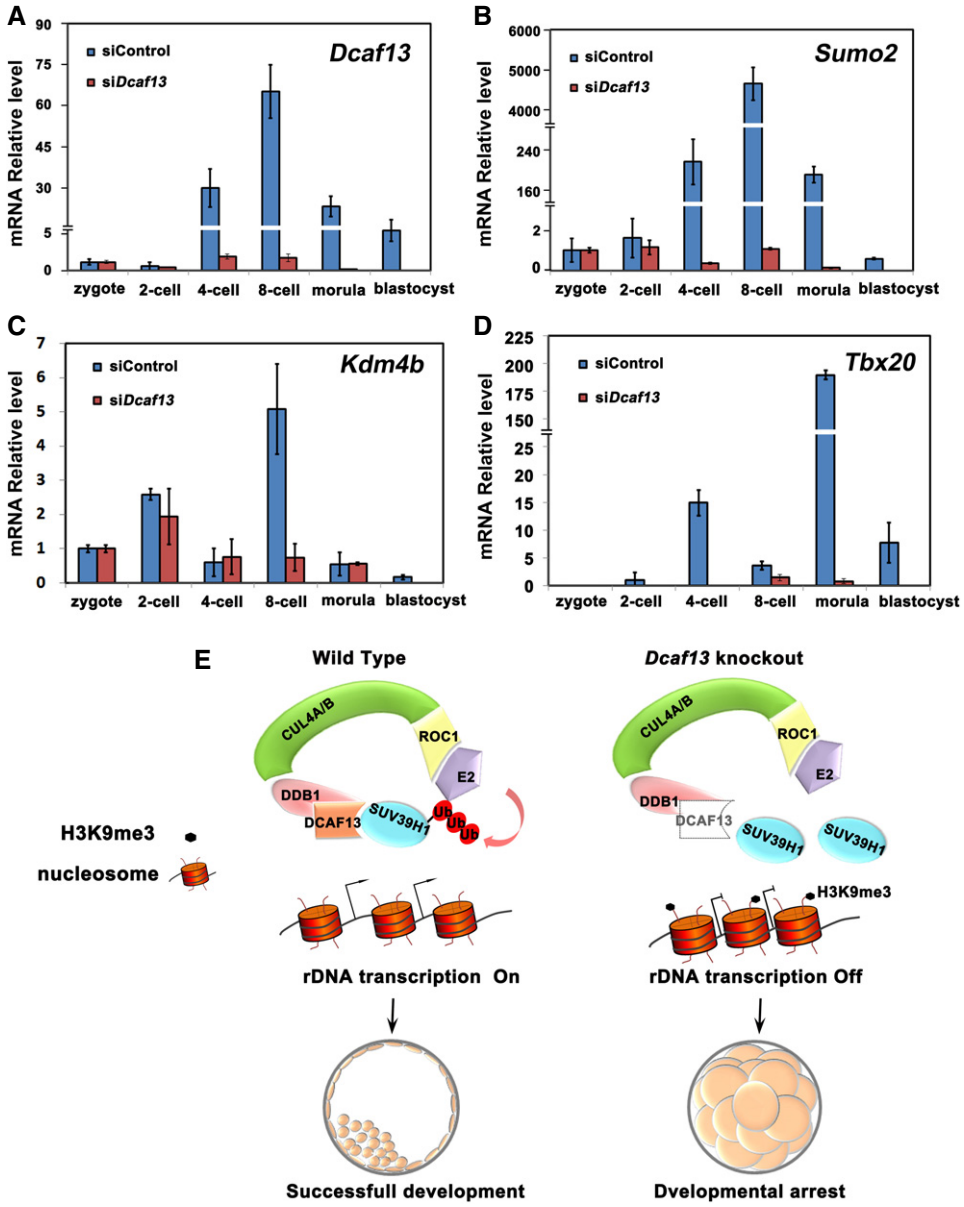

Figure 7. DCAF13 is required for the expression of selective early zygotic genes during preimplantation embryo development.

A–D Quantitative RT–PCR result of *Dcaf13*, *Kdm4b*, *Sumo2*, and *Tbx20* expression in mouse preimplantation embryos after microinjection of siControl or si*Dcaf13* at the zygotic stage. Expression levels at each developmental stage were normalized to *Gapdh*, which served as an internal control. The relative mRNA level in zygote was defined as 1.0. The indicated fold changes at each developmental stage are presented as mean ± SD (n = 3; 30 embryos were collected at each time point).

E A working model explaining how DCAF13 affects establishment of pluripotency during early embryonic development. In preimplantation embryos, SUV39H1 is polyubiquitinated by $CRL4^{DCAF13}$ and destabilized. This mechanism leads to maintenance of H3K9me3 at a low level in specific genomic loci. Active transcription subsequently ensures successful development from the eight-cell to blastocyst stage and establishment of pluripotency. When DCAF13 was knocked out, SUV39H1 could not be polyubiquitinated and became stabilized, resulting in high levels of H3K9me3 in genomic loci and transcription repression. Consequently, pluripotency establishment failed and arrest of the early embryonic development took place.

Therefore, it is spatially possible for DCAF13 to form a complex with CRL4 and recruit some nucleolar proteins for polyubiquitination and degradation.

DCAF13 depletion did not lead to DNA damage and apoptosis as did the knockdown of DDB1 or other well-known CRL4 adaptors (DCAF1 and DCAF2, for example; Pan *et al*, 2013). Instead, SUV39H1 and histone H3K9me3 levels increased in the DCAF13-depleted cells. There are strong connections between nucleolar functions and SUV39H1-mediated histone modifications. It has been reported that in cell lines, the nutrient-dependent or energy-dependent rDNA transcription is controlled by SUV39H1-mediated H3K9 trimethylation (Murayama *et al*, 2008). SUV39H1 has been found to be localized to the periphery, or within the nucleolus, and to participate in the formation of the nucleolar boundary. The fully grown oocyte and zygotes contained a transcriptionally inactive and structurally distinct nucleolar precursor body (NPB;

© 2018 The Authors

Fulka & Langerova, 2014). The zygotic NPB undergoes structural and functional transition to form somatic nucleoli during preimplantation development (Vogt *et al*, 2012; Fulka & Aoki, 2016). Particularly, the perinucleolar heterochromatin rings are tightly associated with NPBs in oocytes and zygotes, as demonstrated by the staining of DNA and epigenetic markers such as HP1 and H3K9me3 (Hamdane *et al*, 2017). Therefore, DCAF13-regulated SUV39H1 stability and H3K9me3 levels may be intimately involved in nucleolus-associated functions. Indeed, rDNA genomic regions showed increased H3K9me3 deposition, and pre-rRNA transcription was repressed in DCAF13-depleted embryos. Because early zygotic rRNA transcription is crucial for preimplantation development, we believe that compromised nucleolar function is one of the major reasons for developmental arrest of *Dcaf13* knockout embryos.

The RNA transcription activity in both nucleolus and nucleoplasm decreased in eight-cell embryos after *Dcaf13* depletion or *Suv39h1* overexpression (EU staining results in Fig 5), indicating that *Dcaf13* is required for general transcription of the embryonic genome. In agreement with this observation, RT–PCR and immunofluorescence staining results in Figs 6 and 7 showed that the expression of key early zygotic genes related to cell linage specification, including *Cdx2*, *Nanog*, and *Kdm4b*, was affected in *Dcaf13*-depleted embryos. Furthermore, because rRNA transcription was repressed by *Dcaf13* depletion, global protein synthesis in blastomeres after ZGA may also be decreased. These combining molecular changes underline the developmental arrest phenotype of *Dcaf13* KO embryos. Although our current study strongly suggests that the increased H3K9me3 level caused the repression of genome transcription activity in preimplantation *Dcaf13* KO embryos, DCAF13 may be involved in transcriptional regulation by targeting other unidentified CRL4 substrates.

This study highlighted the mechanism where $CRL4^{DCAF13}$ mediates SUV39H1 degradation and ensures genome reprogramming in preimplantation embryos, as illustrated in Fig 7E. It is conceivable, however, that the dysregulation of SUV39H1/2 and H3K9me3 is an important, but not the ONLY mechanism that causes preimplantation lethality of *Dcaf13* KO embryos. Some people may argue that the deletion of DCAF13 has much broader general effect on cell physiology. Nevertheless, this opinion is not a justified reason to prevent us from investigating the regulation of H3K9me3 by DCAF13 in preimplantation development. In fact, the "broader general effect on cell physiology" is contributed by multiple specific biochemical events, including the epigenetic changes that we elucidated in this study. $CRL4^{DCAF13}$ may have other substrates in early embryos. As an evolutionarily conserved nucleolar protein, DCAF13 may also have CRL4-independent functions. For example, we observed that the nucleolar localization of endogenous B23 decreased in DCAF13 knockout blastomeres. These are important open questions that are worthy of follow-up studies.

Materials and Methods

Mice

Wild-type ICR strain mice were obtained from the Zhejiang Academy of Medical Science, China. All mutant mouse strains had an ICR background. Mice were maintained under SPF conditions in a controlled environment of 20–22°C, with a 12/12-h light and dark cycle, 50–70% humidity, and food and water provided *ad libitum*. Animal care and experimental procedures were conducted in accordance with the Animal Research Committee guidelines of Zhejiang University. The experiments were randomized and were performed with blinding to the conditions of the experiments. No statistical method was used to predetermine sample size.

Construction of transcription activator-like effector nuclease (TALEN) expression vectors targeting mouse *Dcaf13*

A target site was identified using the online software published by Cermak *et al* (http://boglabx.plp.iastate.edu/TALENT/help.php; Cermak *et al*, 2011). Nucleotide-recognizing TALE single unit vectors and TALEN expression vectors were kind gifts from Bo Zhang (Peking University). TALE repeat arrays and TALE nuclease expression vectors were constructed as described (Qiu *et al*, 2013).

In vitro transcription and preparation of mRNAs for microinjections

To prepare mRNAs for microinjection, expression vectors were linearized and subjected to phenol/chloroform extraction and ethanol precipitation. The linearized DNAs were transcribed using the SP6 mMessage mMachine kit (AM1450; Invitrogen) according to the manufacturer's instructions. mRNAs were recovered by lithium chloride precipitation and resuspended in nuclease-free water.

Microinjection

Mouse zygotes were obtained by superovulation of 7- to 8-week-old females mating with males of the same strain. All injections were performed using an Eppendorf TransferMan NK2 micromanipulator. Denuded zygotes were injected with 5–10 pl samples per zygote. After injection, zygotes were washed and cultured in KSOM (Millipore) at 37°C with 5% CO_2.

For *Dcaf13* knockout, 40 ng/μl mRNA of each TALEN pair was injected into the cytoplasm of zygotes with well-recognized pronuclei, in M2 medium (Sigma). Injected zygotes were transferred into pseudopregnant FVB/N female mice (15–25 zygotes per mouse) after 2 h recovery culture in KSOM.

Founder identification, TA cloning, and sequencing

Tail clips were subjected to standard DNA extraction procedures. For identification of *Dcaf13* mutated founders, the extracted DNA was amplified using GT-F and GT-R primers (Appendix Table S1) flanking the target sites to produce amplifications of 451 bp. The amplified DNA fragments were digested with *Alu* I, and those resistant to *Alu* I digestion were subjected to TA cloning and sequencing.

To identify exact genomic DNA modifications in founders, PCR products from each mutated founder were cloned using a TA cloning kit (Takara) according to the manufacturer's instructions. At least six colonies were picked from each transformation and sequenced.

 © 2018 The Authors

The founder mice were crossed to WT mice for three generations to avoid potential off-target effects due to TALEN-mediated DNA editing. The *Dcaf13* null allele was effectively passed between generations.

Superovulation and fertilization

For superovulation, 21- to 23-day-old female mice were intraperitoneally injected with 5 IU of pregnant mare serum gonadotropin (PMSG; Ningbo Sansheng Pharmaceutical Co., Ltd., P.R. China). After 44 h, mice were injected with 5 IU of human chorionic gonadotropin (hCG; Ningbo Sansheng Pharmaceutical Co., Ltd., P. R. China) and mated with adult males. Successful mating was confirmed by the presence of vaginal plugs. Embryos were harvested from oviducts at the indicated times post-hCG injection.

Confocal microscopy for mouse oocytes and embryos

Oocytes and embryos were fixed in PBS-buffered 4% paraformaldehyde (PFA) for 30 min at room temperature, followed by permeabilization with 0.2% Triton X-100. After blocking with 1% BSA in PBS, oocytes were incubated with primary antibodies diluted in blocking solution at room temperature for 1 h. After three washes with PBS, oocytes were labeled with secondary antibodies for 45 min, and then counterstained with 5 μg/ml of 4′,6-diamidino-2-phenylindole (DAPI) or propidium iodide (PI; Molecular Probes®; Life Technologies, Corp., Carlsbad, CA, USA) for 10 min. Oocytes were mounted on glass slides using SlowFade® Gold antifade reagent (Life Technologies) and examined under a confocal laser scanning microscope (Zeiss LSM 710; Carl Zeiss AG, Germany).

Cell culture, plasmid transfection, and immunoprecipitation

HeLa cells were from American tissue culture collection and grown in DMEM (Invitrogen) supplemented with 10% fetal bovine serum (FBS; HyClone) and 1% penicillin–streptomycin solution (Gibco) at 37°C in a humidified 5% CO_2 incubator. Cells were in healthy conditions but were not tested for mycoplasma contamination.

Mouse *Dcaf13* cDNAs were PCR-amplified from a mouse ovarian cDNA pool and cloned into pCS2- or pcDNA-based eukaryote expression vectors. SUV39H1 clone was picked out from the ORF library of human and cloned into an N-terminal MYC- or mCherry-tag vector. The AD (NHSC to NLAA) mutant of SUV39H1 was generated by mutagenesis PCR and confirmed by sequencing. The lentivirus-based plasmids employed for iPS cell derivation include doxycycline-inducible TetO-FUW-*Oct4*, *Sox2*, *Klf4*, *c-Myc*, and *Cre* plasmids, and the packaging plasmids ps-PAX-2 and pMD2G. Lentivirus was prepared by co-transfection of TetO-FUW plasmids with ps-PAX-2 and pMD2G into 293T cells, and viral supernatant was harvested at 48 h after transfection.

Transient plasmid transfection was done using Lipofectamine 2000 (Invitrogen). Cells were lysed in lysis buffer (50 mM Tris–HCl, pH 7.5, 150 mM NaCl, 10% glycerol, and 0.5% NP-40; protease and phosphatase inhibitors were added prior to use) at 48 h after transfection. After centrifugation at 12,000 *g* for 10 min, the supernatant was subjected to immunoprecipitation with different affinity gels (Sigma) for 4 h at 4°C and washed three times with lysis buffer. SDS sample buffer was added to the beads, and the eluates were used for Western blot analysis. Nucleoli isolation from HeLa cells was conducted as described previously (Andersen *et al*, 2002).

RNA isolation and real-time RT–PCR

Total RNA was extracted using RNeasy Mini kit (Qiagen) according to the manufacturer's instructions. Real-time RT–PCR analysis was performed using a Power SYBR Green PCR Master Mix (Applied Biosystems, Life Technologies) and an Applied Biosystems 7500 Real-Time PCR System. Relative mRNA levels were calculated by normalizing to the levels of endogenous β-actin mRNA (internal control) using Microsoft Excel®. The relative transcript levels of samples were compared to the control, and the fold changes are demonstrated. For each experiment, qPCR reactions were done in triplicate. Primer sequences are listed in Appendix Table S1.

Single-embryo RT–PCR

This method is modified from the RNA Smart-seq protocol reported previously (Picelli *et al*, 2014). Briefly, eight-cell embryos were collected from oviducts of $Dcaf13^{+/-}$ female mice crossed with adult $Dcaf13^{+/-}$ male mice. Each embryo was lysed in 2 μl lysis buffer (0.2% Triton X-100 and 2 IU/μl RNase inhibitor) followed by reverse transcription with the SuperScript III reverse transcriptase and amplification by PCR for 10 cycles. The PCR products were diluted and used for the templates of RT–PCR. Primer sequences are listed in Appendix Table S1.

In vivo ubiquitination assays

FLAG-SUV39H1, MYC-DCAF13, MYC-DDB1 or siRNAs for *Dcaf13* or *Ddb1* were co-expressed with HA-ubiquitin in HeLa cells for 48 h. Lysates were prepared with complete cell lysis buffer (2% SDS, 150 mM NaCl, 10 mM Tris–HCl, pH 8.0, 2 mM Na_3VO_4, 50 mM NaF), followed by addition of dilution buffer (10 mM Tris–HCl, pH 8.0, 150 mM NaCl, 2 mM EDTA, 1% Triton). Lysates were immunoprecipitated with FLAG-M2 beads and analyzed by Western blot with anti-HA antibody. Sequences of control siRNA and siRNAs targeting *Dcaf13* or *Ddb1* are described in Appendix Table S1.

ChIP assay

A modified ultra-low-input ChIP (ULI-NChIP) protocol was followed as previously reported (Brind'Amour *et al*, 2015). Briefly, one hundred eight- to twelve-cell embryos were used per reaction, and two replicates were performed for each treatment. *Zona pellucida* was removed from embryos in acidic Tyrode's solution (Sigma). One microgram of rabbit IgG (PP6421-K; Millipore) or histone H3K9me3 antibody (ab8898; Abcam) was used for each immunoprecipitation reaction. About 10% of whole cell lysis was taken out for input, and the remaining was for ULI-NChIP. The input and immunoprecipitated DNA fragments were purified and subjected to RT–PCR. The status of H3K9me3 on rDNA loci after ChIP was represented as enrichment relative to 10% input. The ChIP assay in HeLa cells was performed using the simple ChIP Enzymatic Chromatin IP

© 2018 The Authors

kit (CST) according to the manufacturer's protocol. The indicated primer sequences and the detailed information of kit used are listed in Appendix Tables S1 and S2, separately.

Western blot analysis

Oocytes or embryos were lysed with SDS sample buffer (100 oocytes or embryos per sample) and heated for 5 min at 95°C. Total oocyte proteins were separated by SDS–PAGE and electrophoretically transferred to PVDF membranes (Millipore Corp., Bedford, MA, USA), followed by blocking in TBST containing 5% defatted milk (BD, Franklin Lakes, NJ, USA) for 30 min. After probing with primary antibodies, the membranes were washed in TBST, incubated with an HRP-linked secondary antibody (Jackson ImmunoResearch Laboratories) for 1 h, followed by three washes with TBST. Bound antibodies were detected using the SuperSignal West Femto Maximum Sensitivity Substrate (Thermo Fisher Scientific Inc., Waltham, MA, USA). The primary antibodies and dilution factors used are listed in Appendix Table S2.

CCK-8 assay

Cell proliferation was determined by cell counting-8 (CCK-8) kit (Dojindo, Kumamoto, Japan) according to the manufacturer's protocol. Briefly, 3,000 cells per well were seed into a 96-well plate with 100 μl DMEM with 10% FBS and cultured for 1–5 days. At indicated time, 10 μl CCK-8 was added into each well and cells were further incubated for 1 h. After incubation, absorbance of OD450 was measured by a microplate reader. By seeding a series of numbers (2000, 4000, 8000, 16000, 32000, 46000) of HeLa cells and measuring OD450 at 6 h once cells adhered to the plate, a standard curve of cell numbers was plotted. The cell number was converted by the OD450 using the standard curve.

EU incorporation assay

Control embryos or embryos injected with siRNAs or mRNAs at indicated time points were cultured in KSOM with 100 μM 5-ethynyl uridine (EU) for 2 h. Fixation, permeabilization, and staining were performed according to the manufacturer's protocol of Click-iT® RNA Alexa Fluor® 488 Imaging kit (C10329; Thermo Fisher Scientific Inc.). Imaging of embryos was acquired on a Zeiss LSM710 confocal microscope.

Statistical analysis

Results are given as means ± SEM. Each experiment included at least three independent samples and was repeated at least three times. Results for two experimental groups were compared by two-tailed unpaired Student's *t*-tests. Statistically significant values of $P < 0.05$, $P < 0.01$, and $P < 0.001$ are indicated by asterisks (*), (**), and (***), respectively.

Expanded View for this article is available online.

Acknowledgements
This study is funded by the National Key Research and Developmental Program of China (2017YFC1001500, 2016YFC1000600, 2017YFC1001100), National Natural Science Foundation of China (31671558, 31741093, 31701260).

Author contributions
H-YF designed this research. Y-LZ, L-WZ, and JZ performed most of the experiments and analyzed data. RL and SG offered reagents and scientific advice. CC and YG performed single-embryo analysis. S-YJ conducted the microinjection experiments in Fig 2. DL injected the zygote and generated the *Dcaf13* founder mice.

Conflict of interest
The authors declare that they have no conflict of interest.

References

Ancelin K, Syx L, Borensztein M, Ranisavljevic N, Vassilev I, Briseno-Roa L, Liu T, Metzger E, Servant N, Barillot E (2016) Maternal LSD1/KDM1A is an essential regulator of chromatin and transcription landscapes during zygotic genome activation. *Elife* 5: e08851

Andersen JS, Lyon CE, Fox AH, Leung AK, Lam YW, Steen H, Mann M, Lamond AI (2002) Directed proteomic analysis of the human nucleolus. *Curr Biol* 12: 1 – 11

Bax R, Vos HR, Raue HA, Vos JC (2006) *Saccharomyces cerevisiae* Sof1p associates with 35S Pre-rRNA independent from U3 snoRNA and Rrp5p. *Eukaryot Cell* 5: 427 – 434

Bosch-Presegue L, Raurell-Vila H, Marazuela-Duque A, Kane-Goldsmith N, Valle A, Oliver J, Serrano L, Vaquero A (2011) Stabilization of Suv39H1 by SirT1 is part of oxidative stress response and ensures genome protection. *Mol Cell* 42: 210 – 223

Brind'Amour J, Liu S, Hudson M, Chen C, Karimi MM, Lorincz MC (2015) An ultra-low-input native ChIP-seq protocol for genome-wide profiling of rare cell populations. *Nat Commun* 6: 6033

Cermak T, Doyle EL, Christian M, Wang L, Zhang Y, Schmidt C, Baller JA, Somia NV, Bogdanove AJ, Voytas DF (2011) Efficient design and assembly of custom TALEN and other TAL effector-based constructs for DNA targeting. *Nucleic Acids Res* 39: e82

Chen J, Liu H, Liu J, Qi J, Wei B, Yang J, Liang H, Chen Y, Chen J, Wu Y, Guo L, Zhu J, Zhao X, Peng T, Zhang Y, Chen S, Li X, Li D, Wang T, Pei D (2013) H3K9 methylation is a barrier during somatic cell reprogramming into iPSCs. *Nat Genet* 45: 34 – 42

Chung YG, Matoba S, Liu Y, Eum JH, Lu F, Jiang W, Lee JE, Sepilian V, Cha KY, Lee DR, Zhang Y (2015) Histone demethylase expression enhances human somatic cell nuclear transfer efficiency and promotes derivation of pluripotent stem cells. *Cell Stem Cell* 17: 758 – 766

Feil R (2009) Epigenetic asymmetry in the zygote and mammalian development. *Int J Dev Biol* 53: 191 – 201

Fulka H, Langerova A (2014) The maternal nucleolus plays a key role in centromere satellite maintenance during the oocyte to embryo transition. *Development* 141: 1694 – 1704

Fulka H, Aoki F (2016) Nucleolus precursor bodies and ribosome biogenesis in early mammalian embryos: old theories and new discoveries. *Biol Reprod* 94: 143

Gu TP, Guo F, Yang H, Wu HP, Xu GF, Liu W, Xie ZG, Shi L, He X, Jin SG, Iqbal K, Shi YG, Deng Z, Szabo PE, Pfeifer GP, Li J, Xu GL (2011) The role of Tet3 DNA dioxygenase in epigenetic reprogramming by oocytes. *Nature* 477: 606 – 610

Hamdane N, Tremblay MG, Dillinger S, Stefanovsky VY, Nemeth A, Moss T (2017) Disruption of the UBF gene induces aberrant somatic

 © 2018 The Authors

nucleolar bodies and disrupts embryo nucleolar precursor bodies. *Gene* 612: 5 – 11

Hannah J, Zhou P (2015) Distinct and overlapping functions of the cullin E3 ligase scaffolding proteins CUL4A and CUL4B. *Gene* 573: 33 – 45

Hatanaka Y, Inoue K, Oikawa M, Kamimura S, Ogonuki N, Kodama EN, Ohkawa Y, Tsukada Y, Ogura A (2015) Histone chaperone CAF-1 mediates repressive histone modifications to protect preimplantation mouse embryos from endogenous retrotransposons. *Proc Natl Acad Sci USA* 112: 14641 – 14646

Herberg S, Simeone A, Oikawa M, Jullien J, Bradshaw CR, Teperek M, Gurdon J, Miyamoto K (2015) Histone H3 lysine 9 trimethylation is required for suppressing the expression of an embryonically activated retrotransposon in Xenopus laevis. *Sci Rep* 5: 14236

Hou Y, Fan W, Yan L, Li R, Lian Y, Huang J, Li J, Xu L, Tang F, Xie XS, Qiao J (2013) Genome analyses of single human oocytes. *Cell* 155: 1492 – 1506

Jansen R, Tollervey D, Hurt EC (1993) A U3 snoRNP protein with homology to splicing factor PRP4 and G beta domains is required for ribosomal RNA processing. *EMBO J* 12: 2549 – 2558

Jia L, Yan F, Cao W, Chen Z, Zheng H, Li H, Pan Y, Narula N, Ren X, Li H, Zhou P (2017) Dysregulation of CUL4A and CUL4B ubiquitin ligases in lung cancer. *J Biol Chem* 292: 2966 – 2978

Jiang Z, Sun J, Dong H, Luo O, Zheng X, Obergfell C, Tang Y, Bi J, O'Neill R, Ruan Y, Chen J, Tian XC (2014) Transcriptional profiles of bovine *in vivo* pre-implantation development. *BMC Genom* 15: 756

Jin J, Arias EE, Chen J, Harper JW, Walter JC (2006) A family of diverse Cul4-Ddb1-interacting proteins includes Cdt2, which is required for S phase destruction of the replication factor Cdt1. *Mol Cell* 23: 709 – 721

Lee J, Zhou P (2007) DCAFs, the missing link of the CUL4-DDB1 ubiquitin ligase. *Mol Cell* 26: 775 – 780

Lee MT, Bonneau AR, Giraldez AJ (2014) Zygotic genome activation during the maternal-to-zygotic transition. *Annu Rev Cell Dev Biol* 30: 581 – 613

Liu W, Liu X, Wang C, Gao Y, Gao R, Kou X, Zhao Y, Li J, Wu Y, Xiu W, Wang S, Yin J, Liu W, Cai T, Wang H, Zhang Y, Gao S (2016) Identification of key factors conquering developmental arrest of somatic cell cloned embryos by combining embryo biopsy and single-cell sequencing. *Cell Discov* 2: 16010

Lu F, Zhang Y (2015) Cell totipotency: molecular features, induction, and maintenance. *Natl Sci Rev* 2: 217 – 225

Ma JY, Ou Yang YC, Wang ZW, Wang ZB, Jiang ZZ, Luo SM, Hou Y, Liu ZH, Schatten H, Sun QY (2013) The effects of DNA double-strand breaks on mouse oocyte meiotic maturation. *Cell Cycle* 12: 1233 – 1241

Matoba S, Liu Y, Lu F, Iwabuchi KA, Shen L, Inoue A, Zhang Y (2014) Embryonic development following somatic cell nuclear transfer impeded by persisting histone methylation. *Cell* 159: 884 – 895

Murayama A, Ohmori K, Fujimura A, Minami H, Yasuzawa-Tanaka K, Kuroda T, Oie S, Daitoku H, Okuwaki M, Nagata K, Fukamizu A, Kimura K, Shimizu T, Yanagisawa J (2008) Epigenetic control of rDNA loci in response to intracellular energy status. *Cell* 133: 627 – 639

Niemann H (2016) Epigenetic reprogramming in mammalian species after SCNT-based cloning. *Theriogenology* 86: 80 – 90

Pan WW, Zhou JJ, Yu C, Xu Y, Guo LJ, Zhang HY, Zhou D, Song FZ, Fan HY (2013) Ubiquitin E3 ligase CRL4(CDT2/DCAF2) as a potential chemotherapeutic target for ovarian surface epithelial cancer. *J Biol Chem* 288: 29680 – 29691

Picelli S, Faridani OR, Bjorklund AK, Winberg G, Sagasser S, Sandberg R (2014) Full-length RNA-seq from single cells using Smart-seq2. *Nat Protoc* 9: 171 – 181

Qiu Z, Liu M, Chen Z, Shao Y, Pan H, Wei G, Yu C, Zhang L, Li X, Wang P, Fan HY, Du B, Liu B, Liu M, Li D (2013) High-efficiency and heritable gene targeting in mouse by transcription activator-like effector nucleases. *Nucleic Acids Res* 41: e120

Rea S, Eisenhaber F, O'Carroll D, Strahl BD, Sun ZW, Schmid M, Opravil S, Mechtler K, Ponting CP, Allis CD, Jenuwein T (2000) Regulation of chromatin structure by site-specific histone H3 methyltransferases. *Nature* 406: 593 – 599

Smith ZD, Meissner A (2013) DNA methylation: roles in mammalian development. *Nat Rev Genet* 14: 204 – 220

Urano T, Shiraki M, Usui T, Sasaki N, Ouchi Y, Inoue S (2010) Identification of non-synonymous polymorphisms in the WDSOF1 gene as novel susceptibility markers for low bone mineral density in Japanese postmenopausal women. *Bone* 47: 636 – 642

Vogt EJ, Meglicki M, Hartung KI, Borsuk E, Behr R (2012) Importance of the pluripotency factor LIN28 in the mammalian nucleolus during early embryonic development. *Development* 139: 4514 – 4523

Xue Z, Huang K, Cai C, Cai L, Jiang CY, Feng Y, Liu Z, Zeng Q, Cheng L, Sun YE, Liu JY, Horvath S, Fan G (2013) Genetic programs in human and mouse early embryos revealed by single-cell RNA sequencing. *Nature* 500: 593 – 597

Yan L, Yang M, Guo H, Yang L, Wu J, Li R, Liu P, Lian Y, Zheng X, Yan J, Huang J, Li M, Wu X, Wen L, Lao K, Li R, Qiao J, Tang F (2013) Single-cell RNA-Seq profiling of human preimplantation embryos and embryonic stem cells. *Nat Struct Mol Biol* 20: 1131 – 1139

Yang JY, Zong CS, Xia W, Wei Y, Ali-Seyed M, Li Z, Broglio K, Berry DA, Hung MC (2006) MDM2 promotes cell motility and invasiveness by regulating E-cadherin degradation. *Mol Cell Biol* 26: 7269 – 7282

Yang Y, Liu R, Qiu R, Zheng Y, Huang W, Hu H, Ji Q, He H, Shang Y, Gong Y, Wang Y (2015) CRL4B promotes tumorigenesis by coordinating with SUV39H1/HP1/DNMT3A in DNA methylation-based epigenetic silencing. *Oncogene* 34: 104 – 118

Yu C, Zhang YL, Pan WW, Li XM, Wang ZW, Ge ZJ, Zhou JJ, Cang Y, Tong C, Sun QY, Fan HY (2013) CRL4 complex regulates mammalian oocyte survival and reprogramming by activation of TET proteins. *Science* 342: 1518 – 1521

Yu C, Ji SY, Sha QQ, Sun QY, Fan HY (2015a) CRL4-DCAF1 ubiquitin E3 ligase directs protein phosphatase 2A degradation to control oocyte meiotic maturation. *Nat Commun* 6: 8017

Yu C, Xu YW, Sha QQ, Fan HY (2015b) CRL4DCAF1 is required in activated oocytes for follicle maintenance and ovulation. *Mol Hum Reprod* 21: 195 – 205

Yu C, Ji SY, Sha QQ, Dang Y, Zhou JJ, Zhang YL, Liu Y, Wang ZW, Hu B, Sun QY, Fan HY (2016) BTG4 is a meiotic cell cycle-coupled maternal-zygotic-transition licensing factor in oocytes. *Nat Struct Mol Biol* 23: 387 – 394

Zhang B, Zheng H, Huang B, Li W, Xiang Y, Peng X, Ming J, Wu X, Zhang Y, Xu Q, Liu W, Kou X, Zhao Y, He W, Li C, Chen B, Li Y, Wang Q, Ma J, Yin Q (2016) Allelic reprogramming of the histone modification H3K4me3 in early mammalian development. *Nature* 537: 553 – 557

Zhu Y, Poyurovsky MV, Li Y, Biderman L, Stahl J, Jacq X, Prives C (2009) Ribosomal protein S7 is both a regulator and a substrate of MDM2. *Mol Cell* 35: 316 – 326

Ziegler-Birling C, Helmrich A, Tora L, Torres-Padilla ME (2009) Distribution of p53 binding protein 1 (53BP1) and phosphorylated H2A.X during mouse preimplantation development in the absence of DNA damage. *Int J Dev Biol* 53: 1003 – 1011

© 2018 The Authors